Structural Engineering and Mechanics, Vol. 30, No. 2 (2008) 147-164
DOI: http://dx.doi.org/10.12989/sem.2008.30.2.147

Numerical modeling for cyclic crack bridging behavior of fiber reinforced cementitious composites

Kyung-Joon Shin†

Department of Civil Engineering Seoul National University, Shillim-dong, Gwanak-gu, Seoul 151-744, Korea

Kwang-Myong Lee‡

Department of Civil and Environmental Engineering SungKyunKwan University, 300 Cheoncheon-dong, Jangan-gu, Suwon 440-746, Korea

Sung-Pil Chang‡†

Department of Civil Engineering Seoul National University, Shillim-dong, Gwanak-gu, Seoul 151-744, Korea

(Received August 9, 2007, Accepted August 8, 2008)

Abstract. Recently, many researches have been done to examine the behavior of fiber reinforced concrete (FRC) subjected to the static loading. However, a few studies have been devoted to cyclic behaviors of FRC. A main objective of this paper is to investigate the cyclic behavior of FRC through theoretical method. A new cyclic bridging model was proposed for the analysis of fiber reinforced cementitious composites under cyclic loading. In the model, non-uniform degradation of interfacial bonding under cyclic tension was considered. Fatigue test results for FRC were numerically simulated using proposed models and the proposed model is achieving better agreement than the previous model. Consequently, the model can establish a basis for analyzing cyclic behavior of fiber reinforced composites.

Keywords: cyclic fiber bridging relation; cyclic constitutive relation; fiber reinforced cementitious composites; numerical modeling.

1. Introduction

Cementitious Composites such as mortar and concrete have been and are still used as the most conventional materials in construction for their workability and remarkable compressive strength. However, the weakness and tendency to be brittle under tension, and particularly fatigue under cyclic loading, remain the largest problem of such cementitious composites.

† Post Doc., E-mail: kj12@snu.ac.kr
‡ Professor, Corresponding author, E-mail: leekm79@skku.edu
‡† Professor, E-mail: spchang@snu.ac.kr

On the other hand, the introduction of fiber-reinforcement is known to improve significantly the tensile behavior of concrete in terms of resistance to fatigue and impact loading as well as tensile strength. Accordingly, fiber reinforced concrete (FRC) has been extensively adopted as cementitious composite for structures likely to be subjected to cyclic loading such as airport pavement, highway overlay, bridge deck and machine foundations (Balaguru *et al.* 1992).

Recently, high performance fiber-reinforced cementitious composites (HPFRCC) such as ECC (Li 2005), SIFCON (Naaman 1991) and DUCTAL (Lafarge) were developed in order to provide high strength or ductility according to the structure at hand. The improved mechanical properties and durability of HPFRCC are promising for future applications to structures exposed to severe loading conditions. However, due to the short history of these new materials, a little is known about the fatigue properties and failure behavior of HPFRCC (Suthiwarapirak *et al*. 2004).

Empirical approach constituted the most common method applied to evaluate fatigue performance. But, this approach requires time-consuming test data collection and processing for a broad range of design cases which, in principle, is not applicable to other design cases (Zhang *et al*. 2000). Therefore, establishing a mechanism-based cyclic bridging model capable to both predict the fatigue life for a given FRC structure and design a FRC material for a given fatigue life as well as for HPFRCC materials is of primary importance. Considerable progress has been realized over the last few years in the area of micromechanics of failure under static loading condition (Li *et al*. 1991, Lin *et al*. 1995, Kanda *et al*. 1999), but a few researches were devoted to cyclic loading condition (Matsumoto *et al*. 1999, Zhang *et al*. 2000, Suthiwarapirak *et al*. 2004). Previous models assumed that the sliding resistance degrades uniformly along the debonded interfaces without accounting for the potential non-uniformity in the degradation process resulting from differences in the relative sliding displacement along the matrix-fiber interfaces.

Accordingly, this research proposes a cyclic fiber bridging model considering the non-uniformity in the degradation of sliding resistance based on micromechanics. To achieve this end, a theoretical model of a single fiber pull-out under cyclic load considering degradation of bond strength as well as Cook-Gordon effect (Cook *et al*. 1964, Bentur 1990) is developed. The bridging models of single fiber are applied for deriving the crack plane bridging model accounting for random orientation and embedded length of fiber.

2. Fiber bridging behavior of FRC under cyclic loading

In order to model the behavior of FRC, the material is classified into un-cracked body and cracked body in engineering views. Before cracking, uncracked body is generally treated as an elastic material, i.e., assumed to be linear elastic in tension up to cracking criteria. After a crack is formed, stress is transferred over the crack by bridging action of fiber (Bentur 1990).

When the embedded fiber is loaded, the fiber is gradually pulled out from the matrix. Pull-out of the fiber is processed by, firstly, a debonding period corresponding to the extension of fiber in a debonding zone followed by fracture of the chemical bond, and then by a sliding period where the debonding zone reaches the embedded end of he fiber causing the entire fiber sliding out of the matrix (Lin *et al*. 1999).

Cyclic fiber bridging exhibits more complicated behavior then such monotonic one as conceptually presented by Wu *et al*. (1994). This behavior is illustrated through Fig. 1 and Fig. 2 with schematic diagrams of the distribution and direction of bond stress under loading/unloading cycles.

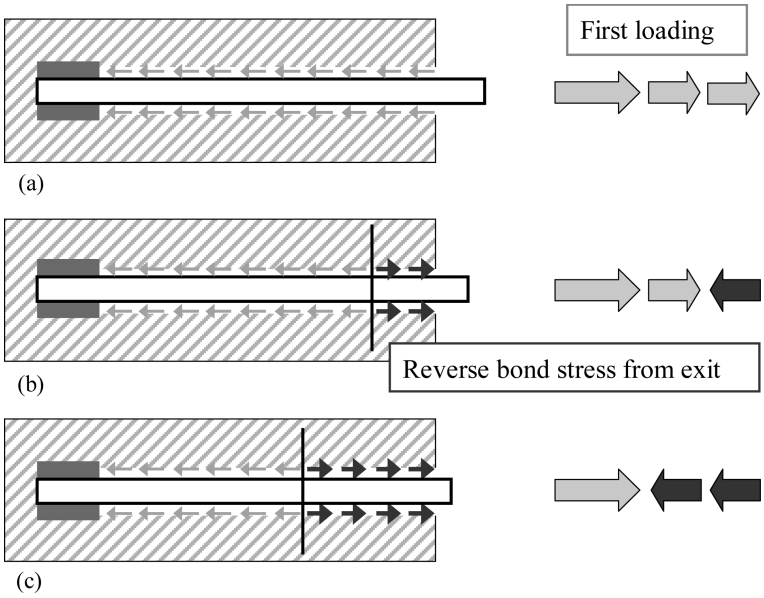

Fig. 1 Distribution and direction of bond stress during unloading processes. (a) first loading, (b) during unloading process, (c) end of unloading

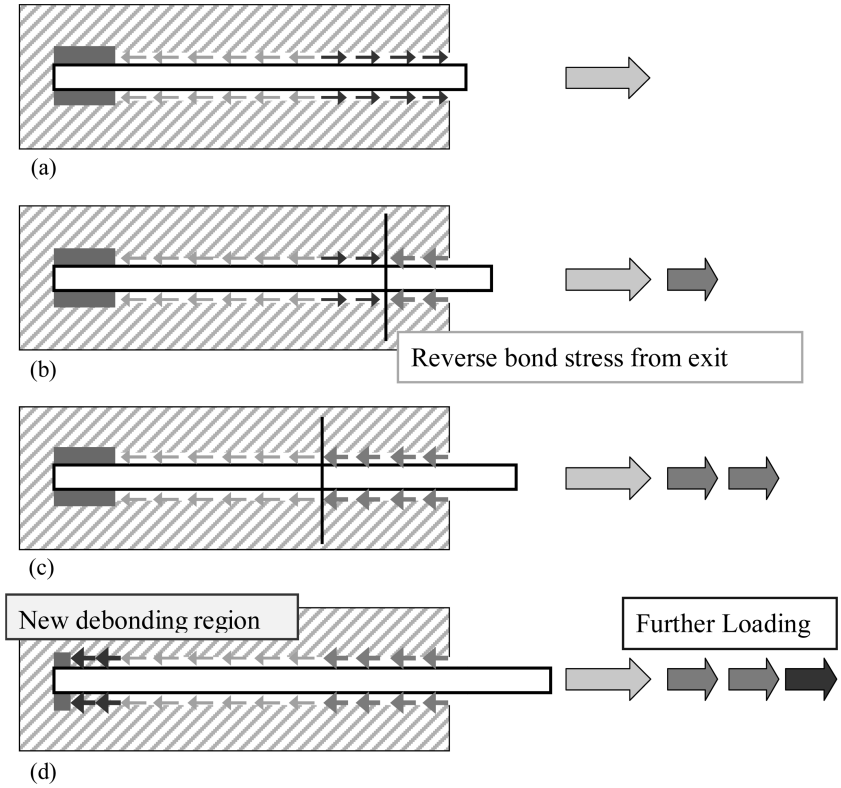

Fig. 2 Distribution and direction of bond stress during reloading process. (a) end of unloading, (b) during reloading process, (c) all reversed bond stress change back again, (d) further loading

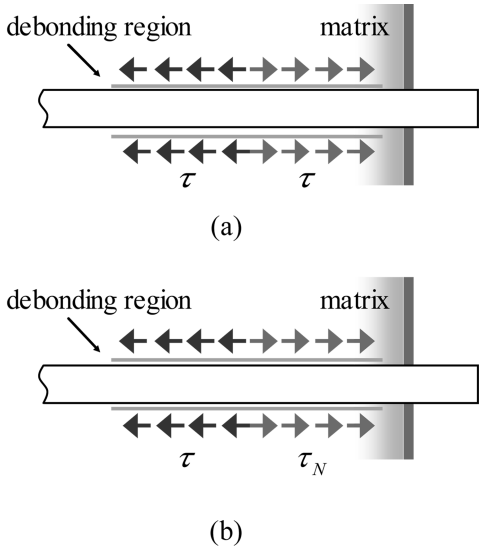

Fig. 3 bond strength distribution of the debonding fiber during unloading

During the first loading cycle shown in Fig. 1(a), the fiber-matrix interface undergoes frictional debonding with gradual extension of the debonding zone as pull-out load is increasing. During the unloading phase following the first loading cycle, the interfacial bond stress of the fiber near the crack plane acts in the opposite direction to resist fiber moving back to the matrix. Figs. 1(b) and (c) picture the gradual extension of the length of reverse stress during the unloading process.

The second loading cycle provokes the gradual shift of the direction of the shear stress along the reversed zone from the exit point toward the embedded end as schematized in Fig. 2(b) until the reverse stress reaches the previous reversed zone as shown in Fig. 2(c). If larger load is applied, a new debonding region will be created to resist the load as illustrated in Fig. 2(d). Subsequent fiber pull-out and slip-back under successive loading/unloading cycles will then progressively smoothen and wear out the interface between fiber and matrix to finally degrade the frictional bond strength. Therefore, the region where the stress act reversely and the region debonded have to be extended with cycles for the case of constant amplitude displacement or loading.

Some models describing this phenomenon have been proposed recently for fiber reinforced cementitious material (Matsumoto *et al*. 1999, Zhang *et al*. 2001, Suthiwarapirak *et al*. 2004). Matsumoto *et al*. (1999) derived a theoretical cyclic bridging constitutive law assuming that the fiber-matrix interface has constant bond strength as shown in Fig. 3(a) degrading with cycles. However, fibers in cyclic loading are gradually pulled out and fiber interface degrades severely near the crack surface, which causes non-uniform degradation of interfacial bond strength. Zhang *et al*. (2001) suggested a semi-analytic crack bridging model for FRC. The authors subdivided the debonding zone into reversal and non-reversal regions as in Fig. 3(b) so as to account for the degradation of bond strength in the reverse stress region. However, the non-uniform degradation between the newly created reverse region and the reverse region created at first unloading could not be considered. Moreover, the proposed model was limited to fiber without chemical bond.

3. Proposed cyclic bridging model

3.1 Scope and model assumptions

As reviewed in the previous chapter, several researchers proposed a cyclic constitutive law describing fiber bridging under cyclic loading based on the micromechanics. However, the previous model failed to consider the non-uniform degradation of bond strength and the chemical bond at the fiber-matrix interface. Accordingly, this paper intends to derive new cyclic bridging constitutive relations including the effect of chemical bond, non-uniform degradation of interfacial bond strength. The newly proposed model expressed in closed equation form also considers pre-debonding effect called Cook-Gordon effect.

The main assumptions adopted in the proposed model are frictional bond strength degradation occurs when the fiber slips in reverse direction, and reverse stress is created from the exit point during unloading/reloading process conceptually presented by Wu *et al*. (1994).

In debonding period, the region where the stress acts reversely in the unloading procedure is continuously increased with the load cycles increases. Therefore, three regions can be assumed according to their behaviors. The one region, the reversal zone, is created at first unloading, and the direction of bond stress continuously changes since the first loading. Therefore, it is assumed that bond strength decreases uniformly with increasing load cycles. Another region, the non reversal zone, is where the direction of bond stress has been not changed. In the non-reversal zone, bond strength is assumed to remain constant because the direction of bond stress is not changed. And the other is the transition zone. As the length of this zone is gradually expanded as the load cycles increases, the non-uniform degradation provoked by the newly created region. In this transition zone, the bond strength near the reversal zone, where is created in early loading stage, undergoes much degradation, whereas the bond strength of newly created transition zone is almost same as the strength of non-reversal zone. Therefore, linear distribution is assumed between the initial and degraded strengths in the transition zone.

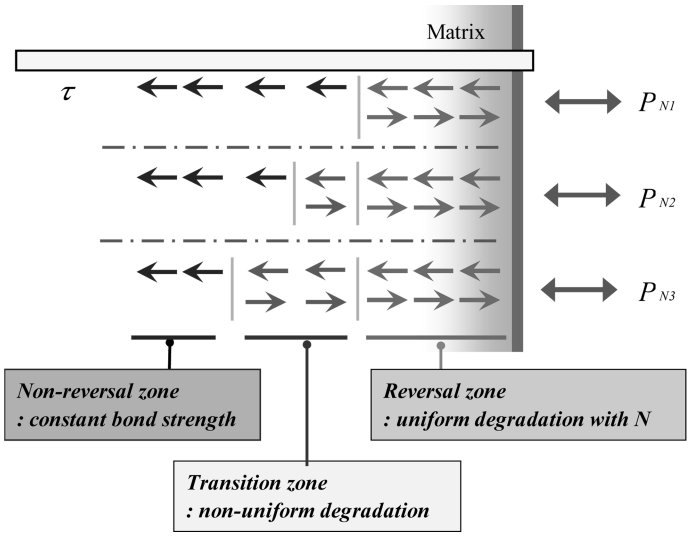

Fig. 4 Assumed bond stress distribution of fiber in debonding period

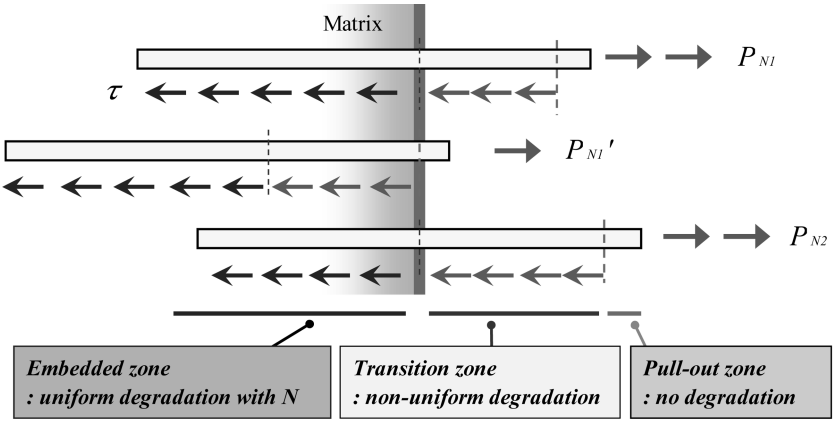

Fig. 5 Assumed bond stress distribution of fiber in pull-out period

In pull-out period, bond stress region is also divided into three regions that are the embedded zone, pull-out zone and transition zone as shown in Fig. 5. In the pull-out region, fiber undergoes pull-out from the matrix at first loading and never slips back into the matrix. Fiber in the embedded region is not experiencing pull-out from the matrix. Therefore, it is assumed that bond strength of embedded zone decreases uniformly with load cycles. In the transition region, fiber undergoes pull-out from the matrix and slip-back into the matrix. Accordingly, the corresponding distribution of bond strength may be non-uniform. Bond strength near the crack plane is stronger than that of deeper embedded region because of larger wearing out during push/pull of fiber. The bond strength is thus assumed to have linear distribution between the embedded and pull-out zones.

3.2 Cyclic bridging model for single fiber in debonding period

3.2.1 First loading stage

The fiber bridging relations during the first loading stage are identical to those of monotonic fiber bridging. For simplicity, Cook-Gordon effect is considered as a pre-debonding at the instant of cracking with assumption that bond strength in pre-debonding region is zero instead of the additional displacement induced by the elastic stretching of the fiber in the pre-debonding region (Li *et al*. 1993). This assumption is illustrated through Fig. 6 showing the distribution of bond strength in fiber.

The pull-out behavior of fiber is generally represented by the relation between pull-out stress, σ_f, and a exit-end slippage, δ, of fiber. The relative pull-out displacement between fiber and matrix in debonding period is calculated as follows (Hsueh 1996, Lin *et al.* 1999, Zhang *et al.* 2001)

$$\delta(x) = \int(\varepsilon_f(x) - \varepsilon_m(x))dx \tag{1}$$

where $\varepsilon_f(x)$, $\varepsilon_m(x)$ are the strain of fiber and matrix at distance x from fiber exit, respectively. Both fiber and matrix are assumed as linear elastic until failure, and the bond strength is assumed as uniform distribution. Also, the end effect and Poisson's effect are neglected. The assumptions can be found detail in Lin *et al.* (1999) and Zhang *et al.* (2001). The proposed models are derived based on the Eq. (1) using newly developed conditions and assumptions.

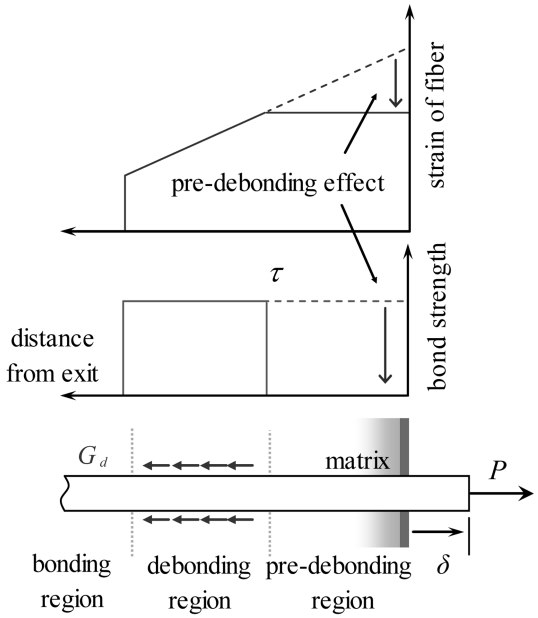

Fig. 6 Fiber pull-out processes in debonding period

Elastic stretching of debonded fiber in pre-debonding region

When the fiber is loaded, the portion of fiber in pre-debonding region slides out frictionally until friction of the whole pre-debonding region is activated. The P-δ relation is given by

$$P = \frac{\pi d_f^2 E_f}{4a_p}\delta \quad \text{for} \quad \delta < \delta_p = \sqrt{\frac{8G_d a_p^2(1+\eta)}{E_f d_f}} = \frac{\sigma_G a_p}{E_f} \tag{2}$$

where δ is the fiber pull-out displacement, a_p is the pre-debonding length, δ_p is the pull-out displacement when all the portion of fiber in pre-debonding region is stretched out, G_d is the chemical bond strength and η is load sharing factor between fiber and matrix, $V_f E_f / V_m E_m$.

Debonding of bonded region

The fiber-matrix interface undergoes debonding which extends the activated fraction of the interfacial zone towards the embedded end of the fiber. The crack opening displacement is given by stretching of the debonded portion of the embedded fiber, and pull-out load increases with the crack opening displacement due to extending debonded interface area. The P-δ relation is given by

$$P = \sqrt{\frac{\pi^2 \tau E_f d_f^3(1+\eta)}{2}\delta + \frac{\pi^2 G_d E_f d_f^3}{2} + \pi^2 \tau^2 a_p^2 d_f^2 (1+\eta)^2} - \pi d_f a_p \tau(1+\eta)$$

$$\text{for} \quad \delta < \delta_{fd} = \frac{2(1+\eta)}{E_f d_f}[\tau(l_e^2 - a_p^2)] + \frac{\sigma_G l_e}{E_f} \tag{3}$$

where τ is the initial bond strength of fiber, δ_{fd} is the fiber pull-out displacement at full debonding and l_e is the embedded length.

3.2.2 General unloading case

Unloading starts once the maximum displacement is achieved. As mentioned previously, a zone where the interfacial stress acts in the reversed direction is created to resist moving back of fiber during unloading. The length of this reversed zone mainly depends on the unloading load and bond strength at the interface.

After a fiber has undergone N times of cycles, the bond stress of fiber is assumed as shown in Fig. 7. When unloading starts, the change of load, ΔP, can be expressed by

$$\frac{\Delta P}{\pi d_f} = \tau_R(x - a_p), \quad \tau_R = (\tau_N + \tau_N')(1 + \eta) \tag{4}$$

and the corresponding change of fiber end slippage, $\Delta\delta$, is calculated using Eq. (1) as following

$$\Delta\delta = \frac{2\tau_R}{E_f d_f}(x^2 - a_p^2) \tag{5}$$

Accordingly, the relation between slippage and force can be expressed as following Eq. (6) by substituting Eq. (5) into Eq. (4).

$$\frac{\Delta P}{\pi d_f} = \sqrt{\frac{\tau_R E_f d_f}{2}\Delta\delta + a_p^2\tau_R^2} - a_p\tau_R \tag{6}$$

where τ_N and τ_N' are the bond and reverse bond strength at N-cycles, respectively. Length of reversal zone at first cycle is x_1. Length of transition zone at N cycles is x_N. Debonding length at N cycles is l_n. This relation holds when reverse stress is created in reversal zone. i.e., $x < x_1$.

When further slippage occurs, the bond stress in the transition zone changes its direction as shown in Fig. 8. In this period, the bridging relation can be calculated by the same method used in Eq. (6).

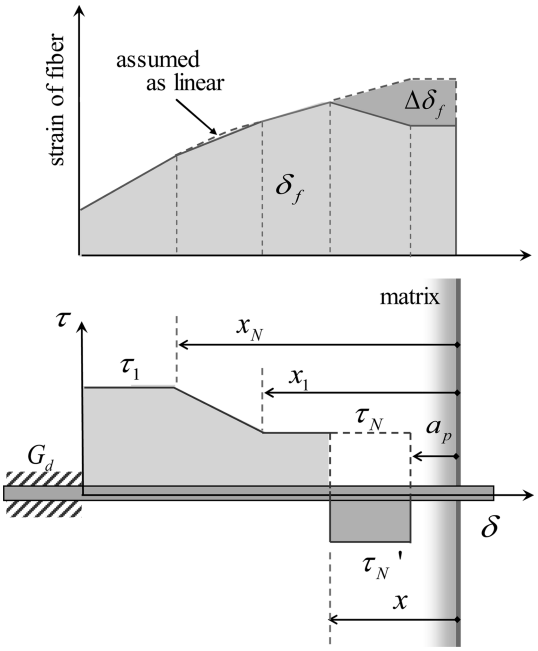

Fig. 7 Reverse stress in reversal zone during unloading

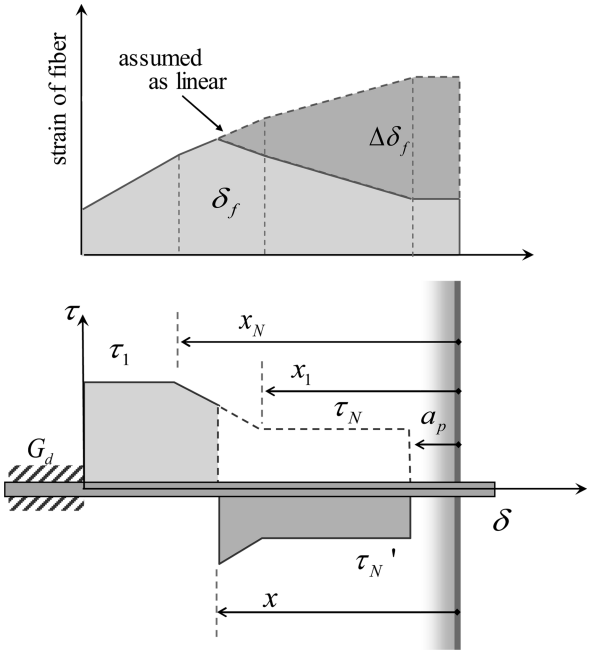

Fig. 8 Stress state of fiber for change of bond stress in transition zone

First, it is derived the relation between the change of force and bond strength and the relation between the change of force and bond strength. Then, the relation between the change of slippage and force can be expressed as

$$\frac{\Delta P}{\pi d_f} = \sqrt{\frac{\tau_T + \tau_R}{4} E_f d_f \Delta\delta + \frac{1}{4}(\tau_T^2 - \tau_R^2)x_1^2 + 2\tau_R(\tau_T + \tau_R)a_p^2} - \frac{1}{2}(\tau_T - \tau_R)x_1 - \tau_R a_p \tag{7}$$

where $\tau_{NR} = (\tau_1 + \tau_1')(1+\eta)$, $\tau_T = \tau_R + (\tau_{NR} - \tau_R)\dfrac{x - x_1}{x_N - x_1}$, τ_1 and τ_1' are the bond and reverse bond strengths at first cycle, respectively. This relation holds for the reverse stress created in the transition zone, i.e., $x_N > x > x_1$.

As bond strength degrades with increasing load cycles, larger reversal zone must be created to attain the minimum slippage (or minimum load). After the change of reverse stress reaches the end of the transition zone, a new reverse stress zone is created as show in Fig. 9, and expressed by

$$\frac{\Delta P}{\pi d_f} = \sqrt{\frac{\tau_{NR} E_f d_f}{2}\Delta\delta + \frac{1}{2}\tau_{NR}(\tau_{NR} - \tau_R)(x_N^2 + x_1^2) + \tau_{NR}\tau_R a_p^2} - \frac{1}{2}(\tau_{NR} - \tau_R)(x_1 + x_N) - \tau_R a_p \tag{8}$$

This relation holds in the newly created reversal zone, i.e., $l_N > x > x_N$.

When the reverse stress reaches the end of debonding region, the stretched fiber contracts because of chemical bond (see Fig. 10). The amount of change in load, ΔP_G, depends on the chemical bond strength, and the relation between change of load and displacement, $\Delta\delta_G$, is calculated by

$$\Delta P_G = \frac{\pi d_f^2 E_f}{4 l_N}\Delta\delta_G \tag{9}$$

Then, the total changes of load, ΔP, and slippage, $\Delta\delta$, are

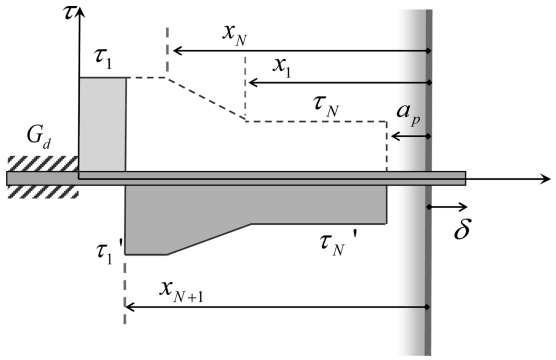

Fig. 9 Stress state of fiber for change of bond stress in non-reversal zone

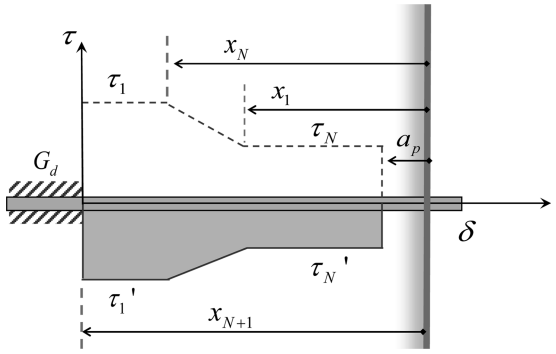

Fig. 10 Stress state of fiber in contracting state

$$\Delta P = \Delta P_L + \Delta P_G, \quad \Delta\delta = \Delta\delta_L + \Delta\delta_G \tag{10}$$

This relation holds for the contracted state of chemical bond, i.e., $x = l_N$, $\Delta\delta_L$ is the change of slippage until $x = l$ and ΔP_L is the change of load until $x = l$.

3.2.3 General reloading

When reloading starts, the direction of the shear stress along the reversed zone gradually changes toward the opposite one. After the end of reversal stress zone reached the previous reversed zone, a new debonding length is created because there is no further reverse shear stress to be created. The relations established for the unloading case remain effective before creation of the new debonding zone.

Due to the degradation of bond strength under cyclic tensile load, the maximum fiber-end slippage or force at reloading period is less than the corresponding value at the last cycle when the length x reaches the end of the reversed stress region. In order to attain the maximum fiber-end slippage or further slippage, pull-out of the fiber has to be larger than that in the previous cycle with a new debonding length being developed as shown in Fig. 11.

The further slippage by new debonding is given by

$$\frac{\Delta P_{ND}}{\pi d_f} = \sqrt{\left(\tau(1+\eta)l_N + \frac{\sigma_G d_f}{4}\right)^2 + \frac{E_f d_f \tau(1+\eta)}{2}\Delta\delta_{ND}} - \tau(1+\eta)l_N - \frac{\sigma_G d_f}{4} \tag{11}$$

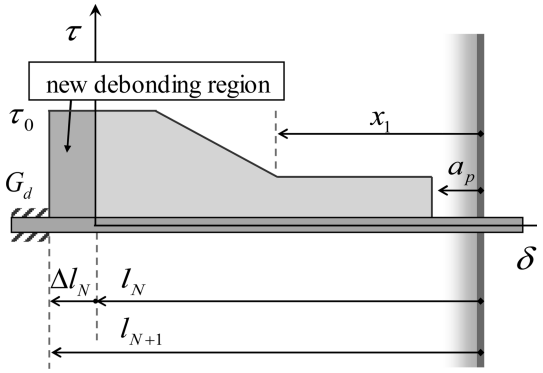

Fig. 11 Stress state of fiber in new debonding state

where l_{N+1}, length of debonding region after reloading, is $l_N + \Delta l_N$, l_N is length of debonding region before reloading, x_N is length of reversal stress region before reloading. ΔP_{ND} is the change of load during new debonding.

3.3 Cyclic bridging relation for single fiber in sliding period

The fiber slides out of the matrix once the debonding length reaches the end of an embedded fiber. The relations between pull-out load and fiber slippage under cyclic load are derived.

3.3.1 First loading case

In this period, the pull-out load is the same as the one of the monotonic loading case (Lin *et al.* 1999). The external load is equilibrated with frictional bond strength of fiber, and expressed as

$$P = \pi d_f [1 + \beta(\delta - \delta_0)/d_f][\tau(l_e - \delta - a_p + \delta_0)] \tag{12}$$

where δ_0 is the fiber end slippage when full debonding is attained, Crack width, w, is 2δ and β is slip-hardening factor. This relation is valid for $\delta < l_e - a_p + \delta_0$. Equations for unloading and reloading are derived based on the Eq. (12).

3.3.2 Unloading case

As in the case of debonding, the direction of the shear stress along the reversed zone gradually changes back. Once the reversal stress reaches the end of embedded fiber, push-in sliding occurs.

During unloading, the direction of bond stress changes back from the exit end of embedded fiber. The relation between load and slippage is the same as the one during unloading of fiber in debonding period.

After complete reversal of the bond stress, the fiber is pushed into the matrix. During the push-back of the fiber, the sliding distance and interfacial bond strength becomes the main contributor of $\Delta\delta$. As mentioned previously, bond strength region is assumed as shown in Fig. 12 during unloading process. Since chemical bond has already been destroyed during debonding period, no need is to consider it in sliding period. Equations for unloading are derived based on the Eq. (12) using these conditions and assumptions. The relation between force and fiber slippage is given by

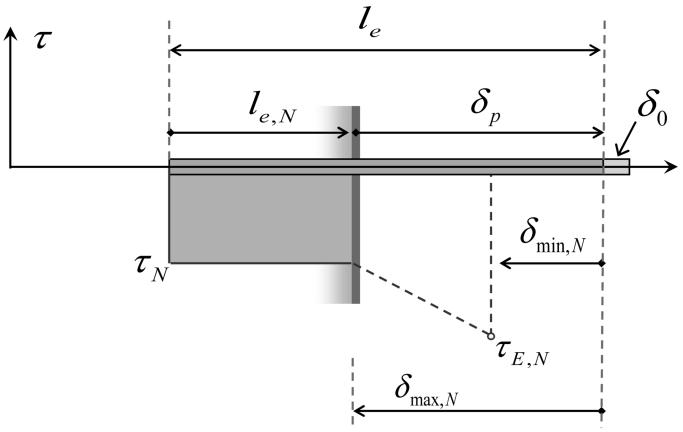

(a) After changing direction of bond stress

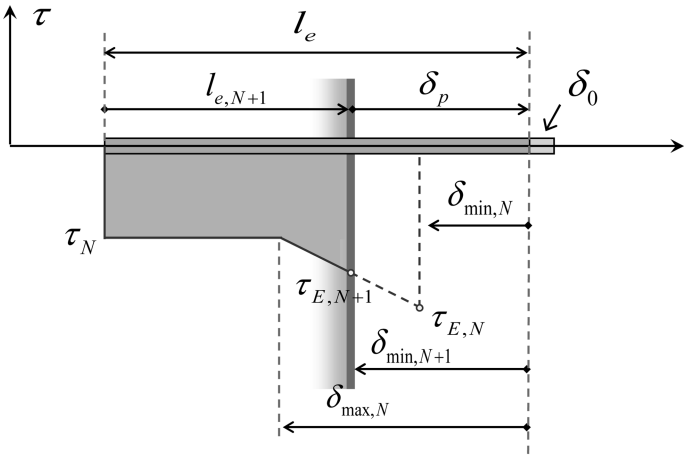

(b) After sliding push-in

Fig. 12 Bond stress of fiber in push-in state

$$P = \pi d_f(1 + \beta\delta_p/d_f)\left(\tau_N(l_e - \delta_p) + \frac{1}{2}(\tau_{E,N+1} - \tau_N)(\delta_{\max,N} - \delta_P)\right)$$

$$\text{for} \quad \delta_{\max,N} > \delta_p > \delta_{\min,N} \tag{13}$$

where δ_p is the slippage in sliding period, calculated by $\delta_p = \delta - \delta_0$. $\tau_{E,N+1}$ is bond strength of fiber at exit-point. When both segments were considered, shorter embedded side is in sliding period and longer embedded side is in debonding period. Therefore crack width w can be calculated by $w = \delta_{debond} + \delta_{slide} = \delta_{debond} + \delta_p + \delta_0$. Although δ_0 and δ_{debond} have been changing continuously during the cyclic loading, amount of slippage by them were relatively small with respect to slippage by total sliding distance. Therefore, it is assumed that δ_0 and δ_{debond} are constant and the same for each other during sliding processes. The change of the bond strength at exit-point during the slide-in process can be expressed as follows.

$$\tau_{E,N+1} = \tau_N + (\tau_E - \tau_N)\frac{\delta_{\max,N} - \delta_p}{\delta_{\max,N} - \delta_{\min,N}} \tag{14}$$

where $\delta_{\max,N}$ and $\delta_{\min,N}$ is the maximum and minimum fiber end slippages at N cycles.

3.3.3 Reloading case

As in unloading case, when reloading starts, the direction of the shear stress along the fiber gradually changes back. After complete change of direction, pull-out sliding occurs. When the slippage is less than maximum value of previous loading as shown in Fig. 13(a), relation between load and slippage is derived as

$$P = \pi d_f (1 + \beta\delta_p/d_f)\left[\tau_N(l_e - \delta_p) + \frac{1}{2}(\tau_{E,N+1} - \tau_N)(\delta_{\max,N} - \delta_P)\right] \tag{15}$$

If slippage exceeds the previous maximum value, fiber in embedded region slides out as the length of embedded fiber decreases as shown in Fig. 13(b). The load in this period is given by

$$P = \pi d_f (1 + \beta\delta_p/d_f)[\tau_N(l_e - \delta_p)] = \pi d_f (1 + \beta\delta_p/d_f)\tau_N l_{e,N+1} \tag{16}$$

where embedded length of fiber, $l_{e,N+1}$, is calculated by $l_e - \delta_p$.

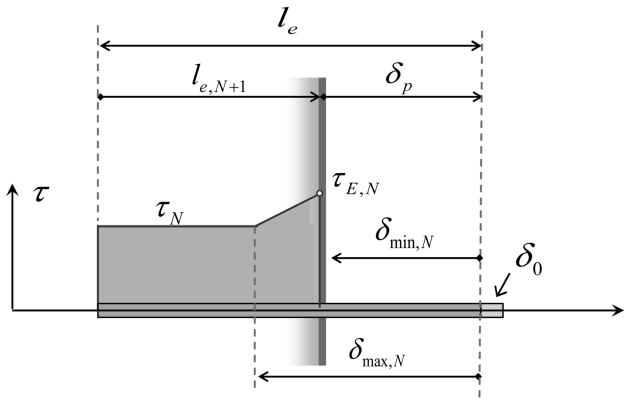

(a) After changing direction of bond stress

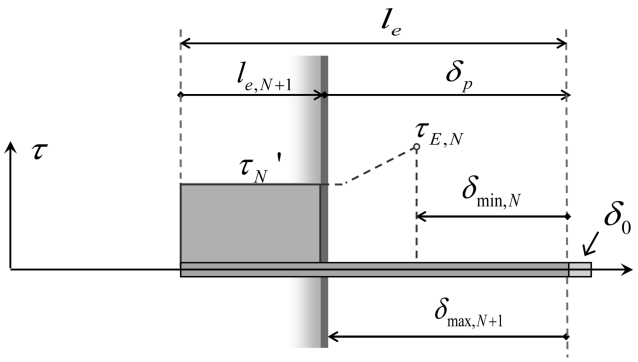

(b) After complete pull-out

Fig. 13 Bond Stress of fiber in pull-out state

3.4 Crack plane model

The crack bridging in fiber reinforced cementitious composite can be obtained by averaging over the contributions of fibers crossing the crack plane. As the constitutive law relates the fiber bridging stress as a function of the crack opening displacement under monotonic loading (Li *et al*. 1991), the bridging stress change-crack opening displacement change relation (Matsumoto *et al*. 1999) is obtained by

$$\Delta\sigma_f = \frac{V_f}{A_f}\int_{\phi=0}^{\frac{\pi}{2}}\int_{z=0}^{\frac{L_f\cos\phi}{2}}\Delta P(l,\phi,\Delta\delta)p(\phi)p(l)dz\,dl \tag{17}$$

where V_f = fiber volume fraction, L_f = fiber length, $p(\phi)$ and $p(l)$ are the probability density functions of the orientation angle and the embedded length.

To account for inclined fiber effect, it is adopted the simple representation that load increases with angle of inclination of fiber (Li *et al*. 1990). This snubbing effect could be represented by the pull-out force of a fiber inclined at an angle (ϕ) by

$$\Delta P(\phi) = \Delta P(\phi=0)e^{f\phi} \tag{18}$$

where f is snubbing coefficient, $\Delta P(\phi=0)$ is a single aligned fiber bridging force derived in section 3.2 and 3.3.

For some fibers, the fiber rupture strength may depend on the inclination angle. In certain high strength synthetic fibers such as PVA, this may be a result of local compression buckling of the bending at the exit point from the matrix. This effect is expressed by strength reduction factor (Kanda *et al*. 1998)

$$\sigma_f^u = \sigma_f^{u'}e^{-f'\phi} \tag{19}$$

where σ_f^u is the reduced strength considering strength reduction factor, $\sigma_f^{u'}$ are the tensile strength of fiber and f' is strength reduction factor.

4. Verification of the proposed model

4.1 Parameters for analysis

To verify the proposed cyclic bridging model, the analytical results are compared with experimental works of Zhang *et al*. (2000, 2001), in which they conducted the cyclic bridging tests of fiber reinforced concrete with 1% volume of steel fiber. Tests were controlled with constant maximum and minimum crack widths. As a result, cyclic crack bridging behavior of fiber reinforced concrete was obtained.

The main object of this study is to propose the model to predict the cyclic bridging behavior with various loading conditions. Therefore, all the analysis is conducted with the same material parameters including the fiber degradation relation. Only the loading conditions (maximum and minimum crack width of loading) are chosen according to the experimental conditions. The proposed cyclic bridging relations are expressed as a function of the pull-out displacement (crack width) and load. Material parameters used in the analysis are shown in Table 1. Because the lack of

Table 1 Material parameters used in the analysis

	Property	Value
Fiber matrix	Fiber Fiber length L_f (mm)	25
	Fiber diameter d_f (mm)	0.4
	Fiber elastic modulus E_f (GPa)	210
	Apparent fiber strength σ_{fu}^{n} (MPa)	1200
	Fiber volume fraction V_f (%)	1
	Matrix elastic modulus E_m (Gpa)	35
Fiber-matrix interface	Friction bond strength τ_d (MPa)	4.9
	Pre-debonding length (mm)	3.0
	Snubbing coefficient f	0.75
Fiber interface degradation	N_0	10
	β_1 (mm^{-1})	10
	β_2 (mm^{-1})	0.7

experimental data for the single fiber under cyclic pull-out load, the degradation parameters are assumed based on the test results of the bridging stress degradation for crack plane.

4.2 Comparison between the analytic and the experimental results

A typical bridging stress-crack width curve during fatigue loading under deformation control is shown in Fig. 14. From this figure, it can be found that the bridging stress at the maximum crack width decreases gradually, whereas bridging stress at minimum crack width increases gradually. Fig. 15 shows stress-crack width relation from the theoretical analysis results obtained by the proposed method. It can be seen that the theoretical results agree well with the experimental ones and describe accurately the characteristics.

Experimental results are normalized with respect to the value at first loading to compare each

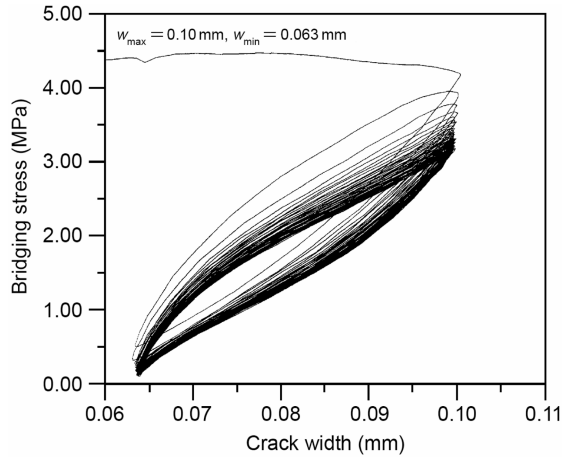

Fig. 14 Typical stress-crack width curve of fatigue test (after Zhang *et al.* 2000)

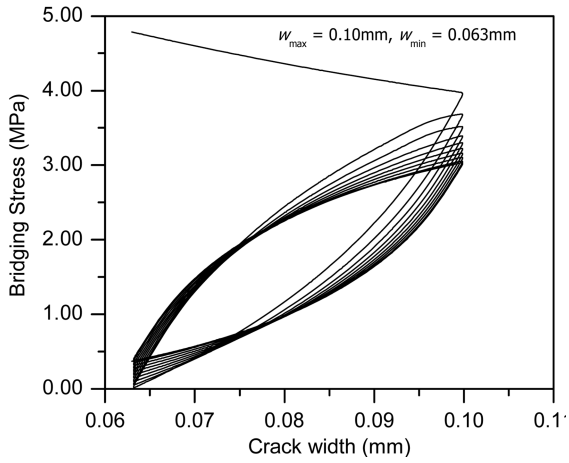

Fig. 15 Stress-crack width curve by the proposed method

other, and given in Figs. 16(a)~(f) as the number of loading cycles. The calculated results are also shown together in Fig. 16. Thick lines represent the analytical results by the proposed model. In the analysis, the same material parameters were used for all case although the maximum and minimum crack widths coincide with the experimental conditions.

From these results, it can be found that these two models successfully simulate the two-stage degradation law of crack bridging observed in the experiments. However the proposed method

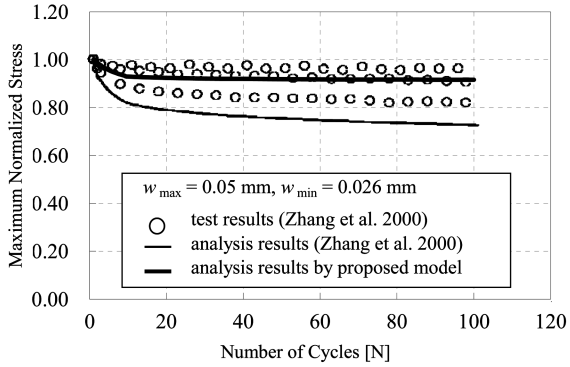

(a) Case for w_{max} = 0.05mm and w_{min}=0.026mm

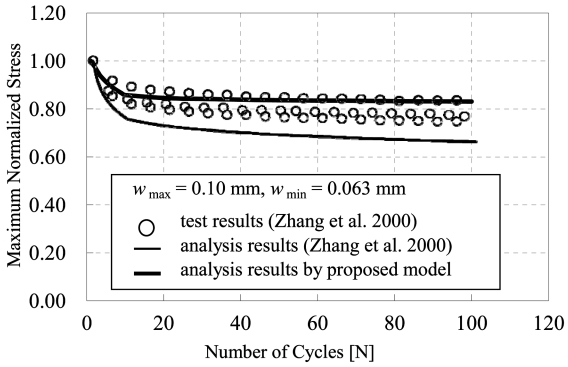

(b) Case for w_{max} = 0.10mm and w_{min}=0.063mm

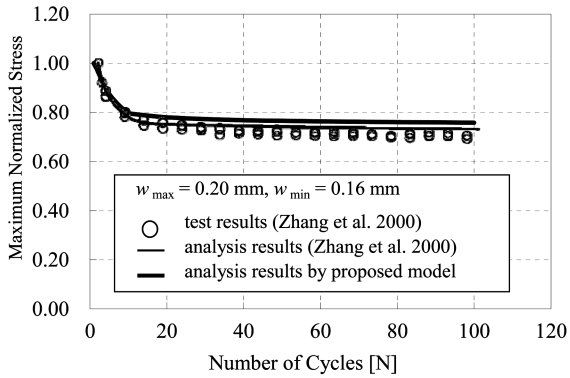

(c) Case for w_{max} = 0.20mm and w_{min}=0.16mm

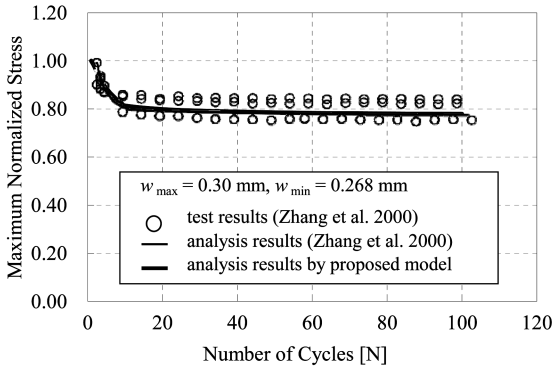

(d) Case for w_{max} = 0.30mm and w_{min}=0.268mm

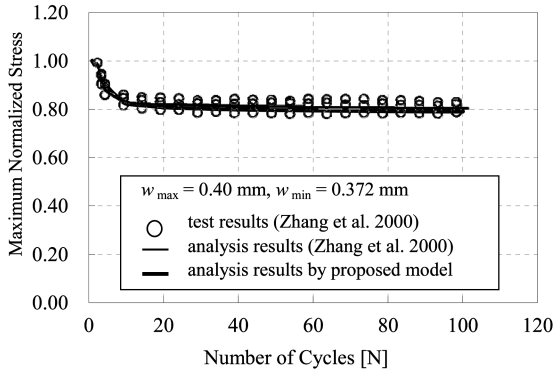

(e) Case for w_{max} = 0.40mm and w_{min}=0.372mm

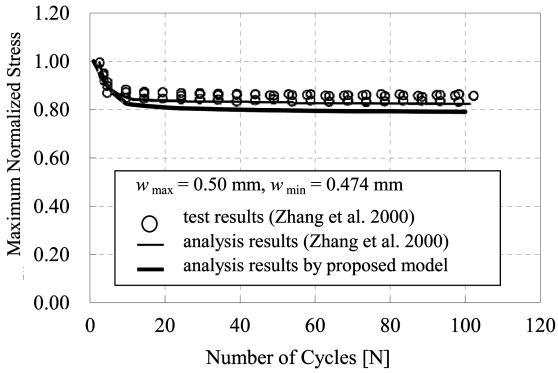

(f) Case for w_{max} = 0.50mm and w_{min}=0.474mm

Fig. 16 Comparison between experimental and analytical results

appears to be in good agreement with the experimental results regardless of the crack width, while the bridging stress theoretically computed by Zhang *et al*. (2001) underestimates the experimental data for the case with small crack width.

The overall bridging behavior of FRC in the small crack width is mainly governed by the debonding behavior of the fibers, and the proportion of the debonding fibers in the matrix decreases as the crack width become larger. Therefore the good agreement for the small crack width may be considered that the proposed model describes the debonding behavior more precisely. However, need is thus for further experimental studies on cyclic behavior of single fiber in order to investigate the effect of individual parameters.

5. Conclusions

A new cyclic bridging model for the analysis of fiber reinforced cementitious composites under cyclic loading has been developed. The developed model was based on the micromechanics which describes the crack bridging stress in short randomly oriented fiber reinforced composites. In the model, non-uniform degradation of interfacial bond strength under cyclic tension has been considered.

The model is based on the assumption that the bond strength of fiber/matrix interfaces is degrading under cyclic loading. In the present model, bond strength in debonding period is divided into three regions; non-reversal zone, transition zone, and reversal zone. The bond strength of reversal zone is assumed as decreasing uniformly. In the transition zone, linear distribution is assumed between the strengths of the reversal and non-reversal zones. In pull-out period, bond strength is also divided into three regions; embedded zone, pull-out zone, and transition zone.

The accuracy of the proposed model was verified through an analytic example. The model is seen to describe the experimental results accurately. Comparison between the analytic predictions and the test results indicate that the proposed model is achieving better agreement than previous model. The adopted methodology is also verified to be capable of simulating fatigue behavior of fiber reinforced cementitious composites. Although further extensive researches are needed such as development of a degradation model as well as verification with large number of experiments, the proposed model can establish a basis for analyzing cyclic behavior of fiber reinforced composites.

References

Balaguru, P. and Surendra, P. (1992), *Fiber-reinforced Cement Composites*, Elsevier.

Bentur, A. and Mindess, S. (1990), *Fiber Reinforced Cementitious Composites*, McGraw-Hill.

Cook, J. and Gordon, J.E. (1964), "A mechanism for the control of crack propagation in all-brittle systems", *Proc. Royal Society*, **A282**, 508-520.

Hsueh, C.H. (1996), "Crack-wake interfacial debonding criteria for fiber-reinforced ceramic composites", *Acta Materialia*, **44**(6), 2211-2216.

Kanda, T. and Li, V.C. (1998), "Interface property and apparent strength of high-strength hydrophilic fiber in cement matrix", *J. Mater. Civil Eng.*, **10**(1), 5-13.

Lafarge, http://www.ductal-lafarge.com

Li, V.C. (2005), "Engineered cementitious composites", *Proceedings of ConMat'05*, Vancouver, Canada.

Li, V.C. and Matsumoto, T. (1998), "Fatigue crack growth analysis of fiber reinforced concrete with effect of

interfacial bond degradation", *Cement and Concrete Composites*, **20**, 339-351.
Li, V.C., Stang, H. and Krenchel, H. (1993), "Micromechanics of crack bridging in fiber reinforced concrete", *J. Mater. Struct.*, **26**, 486-494.
Li, V.C., Wang, Y. and Backer, S. (1991), "A micromechanical model of tension-softening and bridging toughening of short random fiber reinforced brittle matrix composites", *J. Mech. Phys. Solids*, **39**(5), 607-625.
Lin, Z., Kanda, T. and Li, V.C. (1999), "On interface property characterization and performance of fiber reinforced cementitious composites", *J. Concrete Sci. Eng.*, RILEM, **1**, 173-184.
Matsumoto, T. and Li, V.C. (1999), "Fatigue life analysis of fiber reinforced concrete with a fracture mechanics based model", *J. Cement and Concrete Composites*, **21**, 249-261.
Matsumoto, T., Chen, P. and Suthiwarapirak, P. (2004), "Effect of fiber fatigue rupture on bridging stress degradation in fiber reinforced cementitious composites", *FRAMCOS-5*, 653-660.
Naaman, A.E. (1991), "SIFCON: Tailored properties for structural performance", *High Performance Fiber Reinforced Cement Composites*, E&Fn Spon.
Suthiwarapirak, P. (2003), "Fracture mechanics based fatigue life analysis of RC bridge slab repair by fiber cementitious materials", *PhD Thesis*, Univ. of Tokyo.
Suthiwarapirak, P. and Matsumoto, T. (2004), "Multiple cracking and fiber bridging characteristics of engineered cementitious composites under fatigue flexure", *J. Mater. Civil Eng.*, **16**(5), 433-443.
Wu, H.C., Matsumoto, T. and Li, V.C. (1994), "Buckling of bridging fibers in composites", *J. Mater. Sci. Lett.*, **13**, 1800-1803.
Zhang, J., Stang, H. and Li, V.C. (2000), "Experimental study on crack bridging in FRC under uniaxial fatigue tension", *J. Mater. Civil Eng.*, **12**(1), 66-73.
Zhang, J., Stang, H. and Li, V.C. (2001), "Crack bridging model for fiber reinforced concrete under uniaxial fatigue tension", *Int. J. Fatigue*, **23**(8), 655-670.